6-2007

Optical Absorption, Depolarization, and Scatter of Epitaxial Single-Crystal Chemical-Vapor-Deposited Diamond at 1.064 μm

Giorgio Turri
University of Central Florida, turrig@erau.edu

Ying Chen
University of Central Florida

Michael Bass
University of Central Florida

Scholarly Commons Citation

Giorgio Turri et al., "Optical absorption, depolarization, and scatter of epitaxial single-crystal chemical-vapor-deposited diamond at 1.064 μm," Optical Engineering 46 (6), 064002, (June 2007). DOI: http://dx.doi.org/10.1117/1.2748044

Optical absorption, depolarization, and scatter of epitaxial single-crystal chemical-vapor-deposited diamond at 1.064 μm

Giorgio Turri
Ying Chen
Michael Bass
University of Central Florida
CREOL—The College of Optics and Photonics
P.O. Box 162700
Orlando, Florida 32816-2700
E-mail: gturri@mail.ucf.edu

David Orchard
QinetiQ Limited
Saint Andrews Road
Malvern, Worcs WR14 3PS
United Kingdom

James E. Butler
S. Magana
T. Feygelson
D. Thiel
K. Fourspring
Naval Research Laboratory Code 6174
4555 Overlook Avenue Southwest
Washington DC 20375

Randle V. Dewees
Jean M. Bennett
Joni Pentony
Samantha Hawkins
Meghan Baronowski
Andrew Guenthner, MEMBER SPIE
Michael D. Seltzer
Daniel C. Harris
Naval Air Systems Command
1900 North Knox Road, Stop 6303
China Lake, California 93555

C. Martin Stickley, MEMBER SPIE
Defense Advanced Research Project Agency/MTO
3701 North Fairfax Drive
Arlington, Virginia 22203

Abstract. Epitaxial single-crystal chemical-vapor-deposited diamond with (100) crystal orientation is obtained from Element Six (Ascot, United Kingdom) and Apollo Diamond (Boston, Massachusetts). Both companies supply 5×5-mm squares with thicknesses of 0.35 to 1.74 mm. Element Six also provides disks with a state of the art diameter of 10 to 11 mm and a thickness of 1.0 mm. The absorption coefficient measured by laser calorimetry at 1.064 μm is 0.003 cm^{-1} for squares from Element Six and 0.07 cm^{-1} for squares from Apollo. One Apollo specimen has an absorption coefficient near those of the Element Six material. Absorption coefficients of Element Six disks are 0.008 to 0.03 cm^{-1}. Each square specimen can be rotated between orientations that produce minimum or maximum loss of polarization of a 1.064-μm laser beam transmitted through the diamond. Minimum loss is in the range 0 to 11% (mean =5%) and maximum loss is 8 to 27% (mean=17%). Element Six disks produce a loss of polarization in the range 0 to 4%, depending on the angle of rotation of the disk. Part of the 0.04 to 0.6% total integrated optical scatter in the forward hemisphere at 1.064 μm can be attributed to surface roughness. © *2007 Society of Photo-Optical Instrumentation Engineers.* [DOI: 10.1117/1.2748044]

Subject terms: diamond; calorimetry; polarization; scattering.

Paper 060877 received Nov. 8, 2006; accepted for publication Dec. 19, 2006; published online Jun. 25, 2007.

1 Introduction

This study assesses optical properties of state of the art epitaxial chemical-vapor-deposited (CVD) single-crystal diamond at a wavelength of 1.064 μm for potential application as a heat spreading element in solid state lasers. Properties of most interest are the calorimetric absorption coefficient, loss of polarization by light passing through the diamond, and optical scatter.

Diamond was manufactured in 2005 by Element Six (Ascot, United Kingdom) and Apollo Diamond (Boston, Massachusetts). Both companies supplied diamond squares with nominal dimensions of 5×5 mm [(100) face] and thickness in the range 0.35 to 1.74 mm. In addition, Element Six provided disks with a state of the art diameter of 10 to 11 mm [(100) face] and thickness of 1.0 mm (Fig. 1).

Laser calorimetry, which was used in this study to measure absorptance (fraction of incident irradiation that is absorbed), is the recommended method for characterizing optical laser components.[1] In this technique, the change in temperature of a specimen is measured as a function of time when the specimen is exposed to a known laser power and after the exposure is ended. Advantages of laser calorimetry include the simplicity of the apparatus and ease of

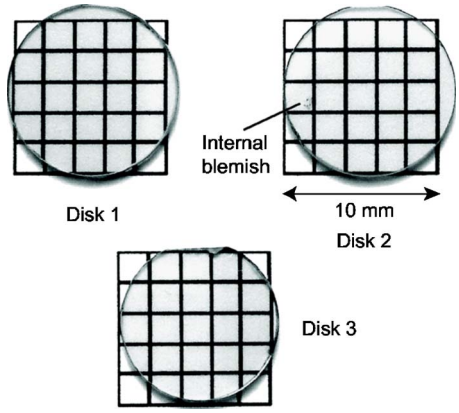

Fig. 1 Diamond disks with a diameter of 10 to 11 mm and thickness of 1.03 to 1.07 mm manufactured by Element Six. The edge of each circle at the top of the photograph was cut flat with a laser and "inspection polished" for attachment of a thermocouple for calorimetry.

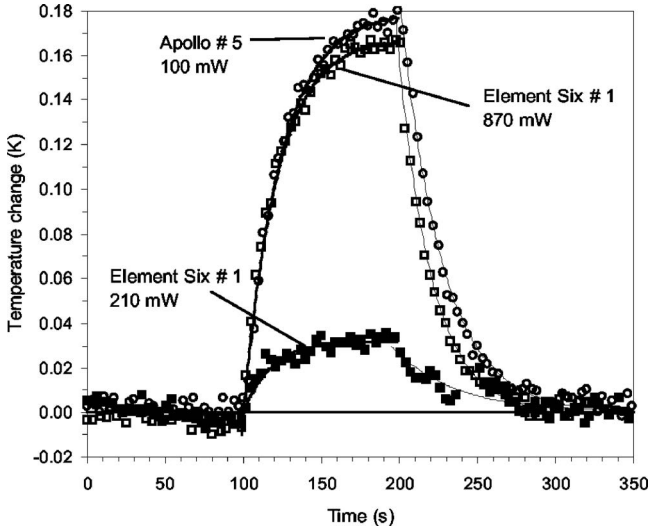

Fig. 2 Irradiation-induced temperature change versus time for Apollo 5 (350 μm thick) and Element Six 1 (430 μm thick) with irradiation time of 100 s. Lines are independent fits to the heating and cooling data with Eqs. (1) and (2) (CREOL data).

absolute calibration. This technique can detect absorptance of the order of a few parts per million.[2] One means to separate surface and bulk absorptance is to study samples with different thicknesses. If the surfaces are identical, then a plot of measured absorptance versus sample thickness extrapolated to zero thickness reveals the surface absorptance. The slope of the graph gives the bulk absorptance.

2 Experimental

2.1 *Laser Calorimetry*

Laser calorimetry was conducted at the University of Central Florida College of Optics and Photonics (CREOL), and independently at QinetiQ (Malvern, United Kingdom). Prior to calorimetry at CREOL, specimens were cleaned with acetone and a cotton bud. Samples were then washed with methanol and wiped with lens paper. After measurement at CREOL, samples were sent to QinetiQ, where they were immersed in concentrated HCl for several minutes and cleaned with a cotton bud. After washing with deionized water and drying with filtered nitrogen, samples were handled at the edges with tweezers.

At CREOL, a styrofoam box was used to enclose the experiment and to provide thermal isolation of the sample at ambient temperature in the air. Laser light entered and exited the box through holes in which plastic tubes were inserted to reduce convective heat transfer. The sample was held by a piece of monofilament fishing line glued to its edge and attached to a thermally isolated frame with three degrees of translational and rotational movement. A precision temperature measurement system by GEC Instruments (Gainesville, Florida) (model S4TC) allowed the simultaneous reading of up to four temperatures with precision better than 10 mK over a broad range. Three 0.2-mm-diameter thermocouples were glued to the sample. Care was taken to prevent scattered laser light from striking the temperature sensors. The overall sensitivity of the calorimeter was about 10 mK.

Lasers emitting TEM_{00} mode light at 1.064 μm used at CREOL to irradiate the samples were 1. a commercial continuous wave Nd:YVO_4 laser with maximum output of 130 mW, or 2. a continuous wave Nd:YAG laser capable of up to 3.5 W. The higher power laser was necessary for the low-loss samples from Element Six. The laser was focused to 1 mm diameter on the entrance surface of the sample. Measurements were made for three different locations in the sample. Examples of the irradiation-induced temperature change versus time are shown in Fig. 2. For each sample and location, ten or more plots were made with irradiation times ranging from 100 to 200 s, and the results averaged.

At QinetiQ, calorimetry was performed in a similar manner with specimens at 300 K in the air.[3] The sample was held by a network of nylon filaments that grip the sample around its edge. Sample temperature was measured by a thermocouple held in contact with the sample edge by one of the filaments. The diode-pumped Nd:YAG laser operated at 1.064 μm with a power of 250 mW. The laser beam at the sample had dimensions of $\sim 0.15 \times 0.34$ mm.

2.2 *Treatment of Calorimetry Data*

Absorptance a is the (dimensionless) fraction of incident radiant power absorbed by a specimen. If the thermal conductivity of the sample is high enough that its temperature (T) is uniform, the temperature variation versus time (t) is given by:

$$\text{during irradiation:} \quad \Delta T(t) = \frac{aP}{\gamma m c_p}\{1 - \exp[-\gamma(t - t_{\text{start}})]\}, \tag{1}$$

$$\text{after irradiation:} \quad \Delta T(t) = \frac{aP}{\gamma m c_p}\{\exp[-\gamma(t - t_{\text{stop}})] - \exp[-\gamma(t - t_{\text{start}})]\}, \tag{2}$$

where m is the mass of the sample (g), P is the incident laser power (W), c_p is the heat capacity of diamond

$[0.51\ \mathrm{J/(g^{*}K)}]$,[4–6] γ is a heat loss coefficient ($\sim 0.02\ \mathrm{s^{-1}}$) determined by fitting the measured temperature versus time, t_{start} is the time at which the sample is exposed to the laser, and t_{stop} is the time at which the exposure is ended. In Eqs. (1) and (2), $\Delta T(t)$ is the difference between the sample temperature at time t and the sample temperature prior to irradiation, which is ambient temperature.

Internal transmittance is the fraction of radiant power that has entered a specimen, which reaches the opposite side after traversing a pathlength b through the specimen. The relation between internal transmittance and absorption coefficient (α) is

$$\text{internal transmittance} = \exp(-\alpha b). \tag{3}$$

Internal transmittance is independent of surface losses by reflection, absorption, and scatter.

For perpendicular incidence of the laser beam on a sample with parallel surfaces, negligible optical scatter, and negligible surface absorption, the absorption coefficient is related to absorptance by

$$\exp(-\alpha b) = \frac{\tau - a}{\tau - Ra}, \tag{4}$$

where τ is the external transmittance and R is the single-surface Fresnel reflectance. When $\alpha b \ll 1$, a first-order expansion of Eq. (4) gives:

$$a \approx \alpha b. \tag{5}$$

If there is surface absorption, a term accounting for both surfaces is added to Eq. (5):

$$a \approx \alpha b + a_{\mathrm{surface}}. \tag{6}$$

For our samples, α ranged between 10^{-1} and $10^{-3}\ \mathrm{cm^{-1}}$ and $b \approx 10^{-1}$ cm, so Eq. (5) applies.

At CREOL, two methods were employed to extract absorptance from the observed temperature versus time. The exponential method[7] consists of fitting the measured data using Eqs. (1) and (2), where a and γ are parameters obtained from a least-squares fit. The gradient method[1,2] consists of taking the derivative with respect to time of the irradiation-induced temperature change versus time at two instants t_h and t_c, during irradiation and after irradiation. For the gradient method, t_h and t_c are chosen so that the temperature change at each instant is the same. From the derivatives taken at these two times, the absorptance is obtained from

$$\frac{d}{dt}\Delta T(t_{\mathrm{h}}) - \frac{d}{dt}\Delta T(t_{\mathrm{c}}) \approx \frac{aP}{mc_{\mathrm{p}}}. \tag{7}$$

The exponential and gradient methods gave similar results, typically disagreeing by less than 5%, when applied to the calorimetry data obtained at CREOL.

The method used to extract absorptance from calorimetry data at QinetiQ has been described previously.[3] Briefly, the heat loss coefficient (γ) and ambient temperature are obtained by fitting the cooling curve. With these values of γ and ambient temperature, the heating curve is fit by using a point-by-point graphical procedure to find absorptance.

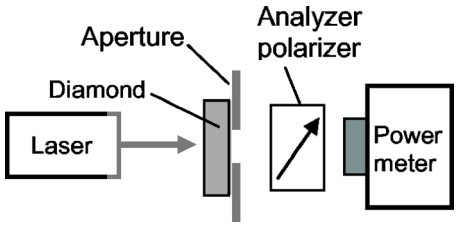

Fig. 3 Setup for measuring loss of polarization.

2.3 *Depolarization Loss*

The apparatus in Fig. 3 was used at CREOL to measure depolarization loss of plane-polarized 1.064-μm radiation from a 127.8-mW $\mathrm{Nd:YVO_4}$ laser. A 3-mm-diam aperture limited the area of the diamond tested. (A 5-mm aperture was used for the diamond disks.) The diameter of the laser beam at the sample was 2 to 3 mm. With no sample present at the aperture, the transmission through the analyzer was 0.887 when it was set to transmit light polarized in the same plane as the laser light, and zero when set to transmit light polarized perpendicular to the laser's polarization.

To make a measurement, the center of the aperture was aligned with the laser beam. The power passing through the diamond P_d was measured with the analyzer polarizer removed. The diamond/aperture combination was rotated about the beam axis to see if the transmission changed. Less than 1.0% variation was observed for the squares from both manufacturers. The more complex behavior of disks from Element Six is described in Results in Sec. 3.

The analyzer polarizer was then inserted and aligned to transmit light polarized parallel to the laser's polarization. The transmitted power P_t was measured for different angles of rotation of the sample about the beam axis. If there were no depolarization loss, P_t should be $0.887P_d$ for all angles. The observed transmitted power was less than $0.887P_d$ and varied as the diamond was rotated. The observed transmitted power was expressed as a percent of transmitted power expected in the absence of depolarization:

$$T = \frac{P_t}{0.887P_d}, \tag{8}$$

and the depolarization loss was defined as $1 - T$.

2.4 *Other Measurements*

A Zygo (Middlefield, Connecticut) GPI-4 Verifire phase measuring interferometer used in a normal Fizeau configuration was employed to measure the flatness of each specimen. Peak-to-valley elevation differences for the inner 90% of the linear dimensions of each sample in Table 1 were obtained from a front surface reflection from each specimen in the air. The tilt aberration term was removed, but was always present in the interferograms. Some results were slightly smoothed with a low-pass filter to remove spikes.

Surface roughness was measured with a Taylor-Hobson (Leicester, United Kingdom) Talystep mechanical profiler equipped with Bennett-Fellows software.[8] The diamond stylus had a hemispheric tip with a radius of 0.8 μm and a loading of 1 mg. Features with lateral dimensions of 2 μm could be resolved. A 1-mm-long profile with 2600 data

Table 1 Diamond optical figure and roughness. Apollo 6 is a 3.6-mm-diam disk. Peak-to-valley elevation difference includes measurements for each of the two optical faces. The outside 5% of pixels from each image was excluded in the peak-to-valley computation. Root-mean-square roughness is the average of three measurements for each of the two optical faces. They were measured by mechanical surface profiler using a stylus with 0.8-μm tip radius and 1-mg loading. Lateral resolution $\approx$2 μm.

Specimen	Thickness (mm)	Peak-to-valley elevation difference (μm)	Root-mean-square roughness (nm)
Squares with nominal dimensions of 5×5 mm			
Element Six 1	0.43	0.18,0.10	—
Element Six 2	0.50	0.14,0.16	—
Element Six 3	0.92	0.12,0.12	—
Element Six 4	1.00	0.17,0.14	1.8±0.4, 0.7±0.2
Element Six 5	1.42	0.17,0.16	—
Element Six 6	1.47	0.18,0.11	—
Apollo 1	0.35	1.40,0.48	—
Apollo 2	0.68	0.28,0.58	2.5±0.2, 5.5±1.6
Apollo 3	1.09	0.82,0.48	2.6±0.3, 2.8±0.2
Apollo 4	1.74	0.19,0.16	—
Apollo 5	0.35	1.44,0.65	—
Apollo 6	1.27	—	—
Disks with diameter 10 to 11 mm			
Element Six disk 1	1.03	0.14,0.21	2.0±0.2, 1.4±0.3
Element Six disk 2	1.07	0.15,0.13	2.4±0.4, 1.3±0.5
Element Six disk 3	1.03	0.13,0.19	3.1±1.5, 2.2±0.4

points was recorded in 32 s, during which instrument drift was negligible. Samples were wiped with folded lens tissue held with tweezers. Inspection with a Nomarski microscope indicated that most of the obvious dust particles were removed with this wipe. Three profiles were taken on each side of each sample. One profile was close to the center, while the other two were on either side and approximately 1 mm away. Profiles with obvious dust peaks were discarded.

Raman spectra were recorded with a Nicolet (Madison, Wisconsin) Fourier Transform Raman 960 instrument with excitation at 1.064 μm, a spot size of $\sim$100 μm, and an InGaAs detector. Resolution was 2 cm^{-1}. The linewidth at half-height of the 1332 cm^{-1} Raman signal (observed at 1.240 μm) for Element Six material was 5 to 7 cm^{-1}. Apollo specimen 4 had a linewidth of 4 cm^{-1}, and Apollo specimen 5 had a linewidth of 11 cm^{-1}. High quality diamond with low strain can have a linewidth as low as 2 cm^{-1}. Ultraviolet spectra were recorded with a Cary (Victoria, Australia) 5 spectrometer using a 2-nm spectral bandwidth and apertures to limit the size of the beam to be less than the size of the diamond specimens. Infrared transmission was recorded with a Nicolet Nexus 870 Fourier transform instrument and with a Nicolet Magna-IR 750 instrument, both with deuterated triglycine sulfate (DTGS) detectors.

Polarized photographs were obtained with a Motic (Xiamen, China) SMZ-143 microscope using polarizers placed directly above and below the specimen. A Leica (Solms, Germany) MEF4 metallograph was used to take differential interference contrast (Nomarski) photographs of diamond surfaces. Polarized and Nomarski micrographs were also obtained with an Olympus (Utsugi, Japan) metallurgical microscope, using a 5× objective.

Photoluminescence was recorded with 532-nm laser excitation illuminating through a metallurgical microscope using a 50× objective with backscattered light analyzed by a Renishaw 2000 spectrometer. The volume of sample illuminated was $\sim$1 μm in diameter and tens of μm deep, while backscattered light was collected from a volume of 1 to 2 μm in diameter and 2 to 3 μm deep. Multiple spectra were recorded on each specimen to survey variability across the sample.

Atomic force microscope images of 50×50-μm squares were obtained with a ThermoMicroscopes (Sunnyvale, California) CP-R microscope in the contact mode using silicon nitride tips.

Total integrated optical scatter in the forward hemisphere between 2.5 and 70 deg from the direction of the incident 1.064-μm laser beam was collected with a Coblentz sphere as described previously.[9] Prior to measuring scatter, samples were cleaned as recommended by Element Six: in a fume hood, 10 mL of 98 wt% H_2SO_4 was heated until white fumes began to evolve. Then 0.5-g KNO_3 was added. A diamond specimen was placed in the hot liquid and left for 10 min. After cooling, the diamond was washed well with distilled water and tipped while in contact with a cotton swab to wick most of the water off, followed by air drying.

3 Results

Epitaxial CVD diamond specimens were clear and colorless or very pale gray, except for Apollo 4, which was gray. Disks from Element Six in Fig. 1 have the largest diameter of epitiaxial single-crystal CVD diamond available to date. An internal blemish, visible to the naked eye, is labeled on disk 2.

Table 1 shows dimensions and surface characteristics of the specimens. Polished faces of Element Six specimens have peak-to-valley elevation differences of 0.1 to 0.2 μm, disregarding rounding at the edges. Apollo specimens have peak-to-valley elevation differences of 0.16 to 1.44 μm. Mechanical surface profile measurements, atomic force microscopy, and Nomarski microscopy indicated that Apollo surfaces were rougher than Element Six surfaces. Roughness measured with a mechanical surface profiler with a lateral resolution of 2 μm is mostly in the range 1 to 3 nm. As measured by atomic force microscopy, a 50×50-μm area of Element Six square 1 had a root-mean-square roughness of 1.2 nm. A corresponding area of Apollo 2 had

Table 2 Calorimetric absorptance, loss of polarization, and forward optical scatter at 1.064 μm. Apollo 6 is a 3.6-mm-diam disk. Transmittance for loss of polarization minimum and maximum is calculated with Eq. (8). Multiple numbers for total integrated forward scatter are from measurements of different locations on the same specimen.

		Calorimetric absorptance (%)		Loss of polarization (%)		
Specimen*	Thickness (mm)	CREOL	QinetiQ	Minimum	Maximum	Total integrated forward scatter (%)
Squares with nominal dimensions of 5×5 mm.						
Element Six 1	0.43	0.015	0.026	3.6	22.4	0.30
Element Six 2	0.50	0.021	0.015	4.1	17.9	0.16
Element Six 3	0.92	0.090	0.113	8.3	26.5	0.15, 0.27, 0.38
Element Six 4	1.00	0.021	0.039	2.6	9.5	0.26
Element Six 5	1.42	0.057	0.042	9.4	21.7	0.04, 0.17
Element Six 6	1.47	0.044	0.041	5.1	17.5	0.08, 0.10
Apollo 1	0.35	—	—			
Apollo 2	0.68	0.32, 0.63	0.55	2.3	11.7	0.33, 0.43
Apollo 3	1.09	0.63, 0.61	0.70	3.6	15.4	0.20, 0.49
Apollo 4	1.74	7.2	—	11.1	21.0	0.11, 0.31
Apollo 5	0.35	0.08, 0.14	0.14	1.3	11.7	0.25
Apollo 6*	1.27	0.069	—	0.0	8.2	
Disks with diameter 10 to 11 mm						
Element Six disk 1	1.03	0.085	0.075	1	4	0.04
Element Six disk 2	1.07	0.32	0.36	0	4	0.63
Element Six disk 3	1.03	0.25	0.28	0	3	0.58

a roughness of 2.6 nm with obvious parallel polishing grooves. Element Six squares appeared smooth under the Nomarski microscope, but small pits were evident in the surfaces of Element Six disks. Plane polarized laser light transmitted through the disks produced interference patterns from which we deduced that the faces of Element Six disks 1, 2, and 3 have wedge angles of 0.007, 0.027, and 0.010 deg, respectively.

3.1 *Absorption and Scatter at 1.064 μm*

Each absorptance in Table 2 is an average of measurements at three to eight locations with standard deviations between locations in the range 5 to 46%. Data from CREOL and QinetiQ are in reasonable agreement. Absorptance versus sample thickness for diamond squares is plotted in Fig. 4. Ideally, the points should lie on a straight line with an intercept of 0 [Eq. (5)] if there is no surface absorption. If there is surface absorption, the y intercept would be a_{surface} [Eq. (6)].

For Element Six squares, the absorptance of specimens 1, 2, 4, 5, and 6 lies near a straight line in Fig. 4. The higher absorptance of specimen 3 is clearly not from the same population. The slope of the line for Element Six in Fig. 4 gives an absorption coefficient of $\alpha=0.0026\pm0.0005$ cm^{-1}. The intercept of 0.006 ± 0.006 implies that there is little surface absorptance.

For Apollo material, a line in Fig. 4 was fit to specimens 3 and 5, plus one of three measurements for specimen 2. The other two measurements for specimen 2 lie above the line. The gray colored sample, Apollo 4, which is not shown on the graph, had much higher absorptance and was clearly not in the same population. Apollo 6, which is shown on the graph, has much lower absorptance than the other samples. The slope of the line for Apollo material in Fig. 4 gives an absorption coefficient of $\alpha=0.071\pm0.005$ cm^{-1} and the intercept is -0.13 ± 0.04. Since surface absorptance cannot be negative, we attribute the negative intercept to variability of the absorptance in the small number of specimens.

Neglecting possible contribution from surface absorption, the mean absorption coefficient of Element Six disks is 0.008 cm^{-1} for disk 1, and 0.03 cm^{-1} for disks 2 and 3. These absorption coefficients are 3 to 10 times greater than that of Element Six squares.

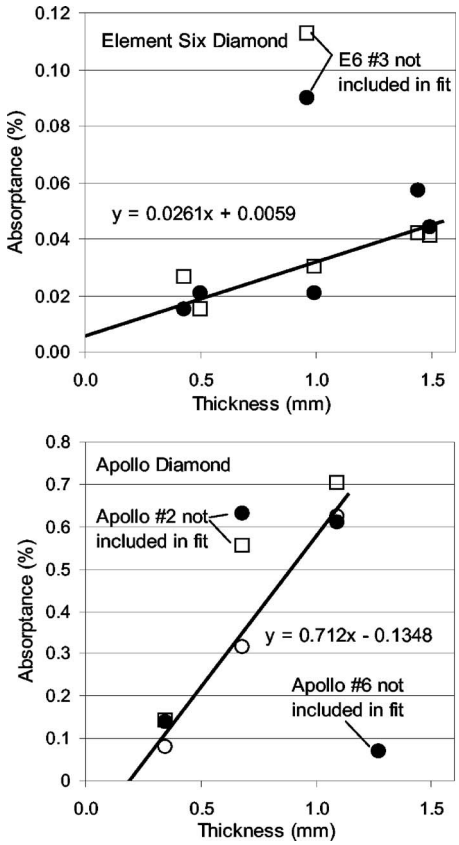

Fig. 4 Absorptance of diamond at 1.064 μm as a function of thickness for Element Six and Apollo diamond squares. CREOL measurements: ○ ●. QinetiQ measurements: □. In the CREOL measurements, open circles were obtained with samples in a Teflon holder and filled circles were obtained with samples held by nylon filaments.

The total integrated forward optical scatter of diamond specimens at 1.064 μm from 2.5 to 70 deg in Table 2 ranges from 0.04 to 0.63%. Element Six reports that forward scatter from their best quality epitaxial single-crystal CVD diamond is $<0.05\%$ at 1.064 μm integrated from 3.5 to 87.5 deg.[10]

3.2 *Loss of Polarization at 1.064 μm*

Figure 5 shows representative photographs of specimens viewed in white light through crossed polarizers. A perfect, isotropic material would appear solid black, because the incident polarization would be blocked by the analyzer polarizer. Features in Fig. 5 arise from rotation of the plane of polarization by strain or defects in the crystal.

Images of disks 1 and 2 in Fig. 6 were made by projecting plane polarized He-Ne laser light (0.6328 μm) through each disk onto a white screen. A polarizer inserted between the sample and the screen was aligned either parallel or orthogonal to the polarization of the incident beam. The image on the screen was captured by a monochrome digital camera. Interference fringes observed in parallel polarization indicate that the faces of disks 1 and 2 have wedge angles of 0.007 and 0.027 deg, respectively [because each fringe arises from a change in thickness of diamond equal to $\lambda/(2n)$, where $\lambda=0.63$ μm and n is the refractive index

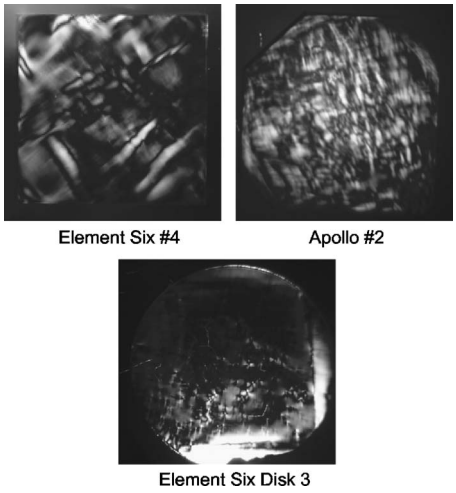

Fig. 5 Representative views of Element Six and Apollo diamond seen with white light through crossed polarizers. Each photograph shows an entire specimen.

≈ 2.4]. The upper right photograph shows little light transmitted through disk 1 with crossed polarizers, indicating that disk 1 produces little loss of polarization. The lower right photograph shows two prominent Maltese cross-features associated with defects that rotate the plane of polarized light. The larger feature, marked by an arrow, corresponds to the internal blemish that is visible to the naked eye in Fig. 1.

The experiment in Fig. 3 quantified the loss of polarization. Different degrees of depolarization were observed as each specimen was rotated about the axis of the laser beam. Table 2 shows the minimum and maximum loss of polarization observed for each sample. The angular separation between minimum and maximum was not 90 deg. Most square specimens had an orientation in which the loss of polarization was less than 5%. Disks from Element Six produced less depolarization. The laser beam used for this measurement was 2 to 3 mm in diameter. The prominent

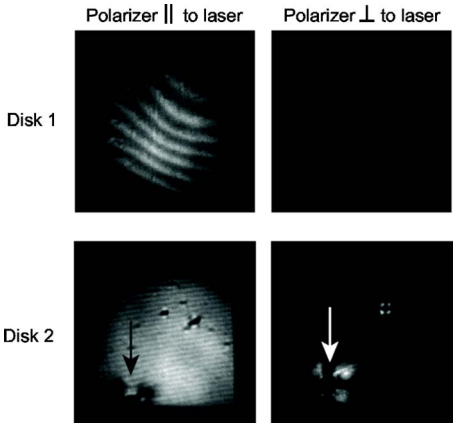

Fig. 6 Projected images of Element Six disks 1 and 2 with 0.6328-μm laser light. Almost the entire disk is seen in each panel. Vertical arrows in the lower images denote the blemish that is visible to the naked eye in Fig. 1.

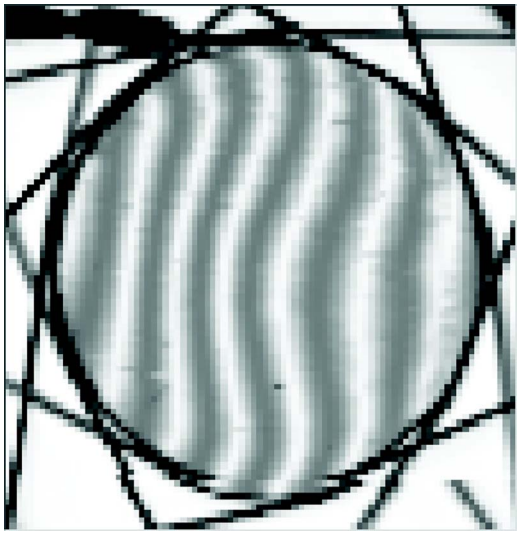

Fig. 7 Map of 1.064-nm transmittance through the entire Element Six disk 1 translated on an *x-y* stage in front of the laser. Transmittance through the diamond varies from ~50 to 100%. Lines outside of the disk are nylon filaments used to support the specimen.

depolarizing defect in the lower right photograph in Fig. 6 may not have been sampled in the quantitative measurement.

The transmission map in Fig. 7, made by translating the specimen on an *x-y* stage in front of the laser beam, confirms the observation of fringes in disk 1 in Fig. 6. Transmittance through the diamond varies from ~50 to 100% in this map. Careful mapping of the disks shows the same modulation period in absorptance that is observed in transmission. None of the square specimens exhibited this modulation.

3.3 *Spectroscopic Characterization*

The ultraviolet absorption of Element Six specimens in Fig. 8 is near the theoretical reflection limit, shown by the dashed line computed from Fresnel reflection calculated with the published refractive index of diamond.[11] That is, there is negligible absorption at wavelengths longer than 236 nm. Apollo squares 1, 2, 3, and 5 exhibit barely detectable absorption in the region 240 to 300 nm, with a peak absorption coefficient of ~2 cm^{-1} at 250 nm. Apollo 4, which is the only gray specimen, has stronger ultraviolet absorption. At shorter wavelengths than the intrinsic absorption edge near 236 nm, the absorption coefficients of all Element Six specimens and Apollo 1, 2, 3, and 5 are nearly identical. The absorption coefficient of 6.5 cm^{-1} at 230 nm is within 10% of the value previously reported for "intrinsic" absorption of diamond.[12]

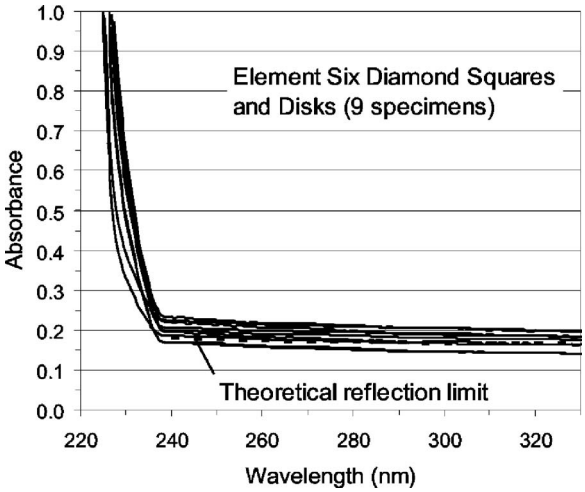

Fig. 8 Ultraviolet absorption of nine Element Six specimens with air in the reference beam. The theoretical reflection limit shown by the dashed line is computed for Fresnel reflection.

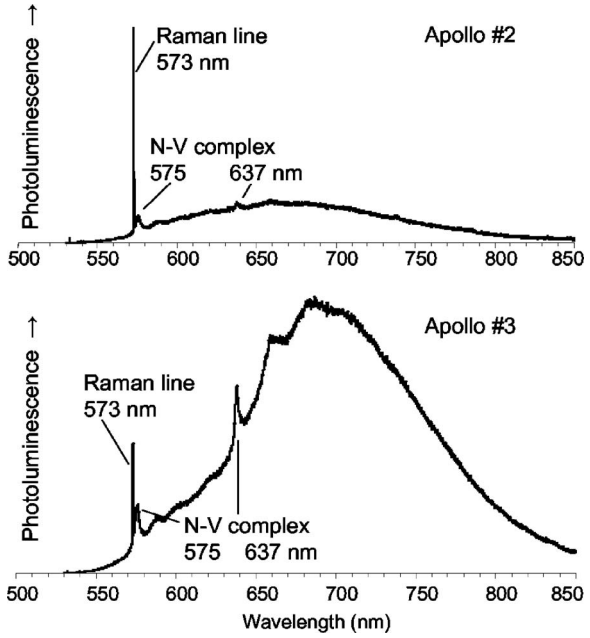

Fig. 9 Photoluminescence from Apollo diamond excited at 532 nm. The two spectra represent the range of different results for Apollo diamond.

Photoluminescence spectra from laser excitation at 532 nm in Fig. 9 represent the range of behavior observed in different samples from Apollo. The spectrum in Fig. 10 is representative of all Element Six squares and disks. The Raman signal in the 532-nm photoluminescence spectra is

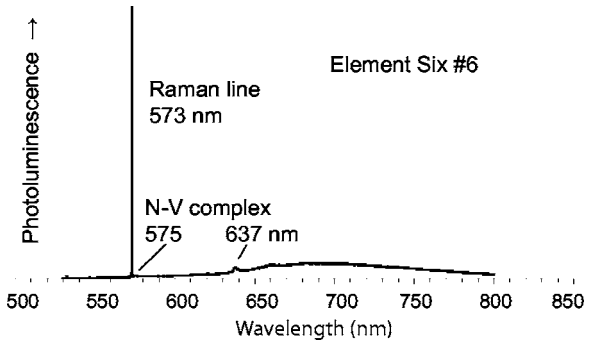

Fig. 10 Photoluminescence from Element Six diamond with excitation at 532 nm. This spectrum is representative of all Element Six diamonds.

located at 573 nm, 1332 cm^{-1} away from the excitation wavelength. Other features of the photoluminescence spectra are described in Sec. 4.

4 Discussion

Extensive reviews of the optical properties of single-crystal natural diamond have been published,[13–17] but most properties are associated with defects and impurities. Single-crystal CVD diamond has been made with high electrical carrier mobility[18] and with excellent optical properties for etalons operating at 1.55 μm.[19] Properties reported by Element Six for their best single-crystal CVD diamond with dimensions of $\sim 4 \times 4 \times 1$ mm include the following:[10]

absorption coefficient at 1.06 μm: <0.01 cm^{-1}
absorption coefficient at 10.6 μm: ~ 0.025 cm^{-1}
forward scatter at 0.63 μm integrated from 0.3 to 45 deg: $<0.03\%$
forward scatter at 1.06 μm integrated from 3.5 to 87.5 deg: $<0.05\%$
forward scatter at 10.6 μm integrated from 1.1 to 45 deg: $<0.0005\%$
thermal conductivity: ~ 2500 W/(m·K)
strength of nine $5 \times 3 \times 0.17$ to 0.35-mm cantilever beams: 1.5 to 5.1 GPa (mean=3.4 GPa, standard deviation=1.3 GPa)
flatness: <0.19 μm
surfaces parallel to ±15 arc sec (0.004 deg).

For polycrystalline CVD diamond, the absorption coefficient of high quality material with a thickness of 0.5 to 1 mm at 10.6 μm is typically 0.03 to 0.07 cm^{-1}.[20–23] The substantial temperature dependence of absorption at 10.6 μm has been explained in terms of multiphonon processes.[24] The optical constants n and k for polycrystalline CVD diamond have been reported for the range 2.5 to 500 μm.[25]

The purpose of the present study was to evaluate optical properties of single-crystal epitaxial CVD diamond at 1.064 μm relevant to its use as a heat spreading element in the optical path of a solid state laser. The absorption coefficient of diamond from Element Six was approximately 0.003 cm^{-1}. Diamond elements with a total thickness of 1 cm in the optical path of a 1.064-μm laser would absorb only 0.3% of the energy of the beam. For Apollo material examined in this study, the absorption would be 7%, but there was one Apollo specimen whose absorption was only twice as great as that of the Element Six material.

Loss of polarization by radiation traversing the solid state laser is a serious issue. We observed varying loss of polarization as diamond squares were rotated about their ⟨100⟩ axis parallel to the path of the laser beam. Table 2 shows that, for most squares from Element Six or from Apollo, there was an orientation in which the loss of polarization was $<5\%$. Disks from Element Six had an optimum orientation in which their loss of polarization was $<1\%$. Even in their worst orientation, loss of polarization from the disks was less than loss from the squares. Our results are qualitatively similar to the range of birefringence observed by van Loon et al.[26]

Optical scatter by material from either manufacturer was in the approximate range 0.04 to 0.6%. The lowest and highest scatter were observed from disks. For surface microirregularities on a well-polished surface, the total integrated scatter from a single surface into one hemisphere is related to the root-mean-square roughness δ and wavelength of light λ by the approximate equation[27]

$$\text{total integrated scatter} \approx \left(\frac{4\pi\delta}{\lambda}\right)^2. \tag{9}$$

A roughness of 2 nm produces a scatter of 0.06% at a wavelength near 1 μm and a roughness of 5 nm produces a scatter of 0.3%. Equation (8) does not apply to scattering caused by scratches, pits, dust particles, contamination, and other isolated blemishes on surfaces.

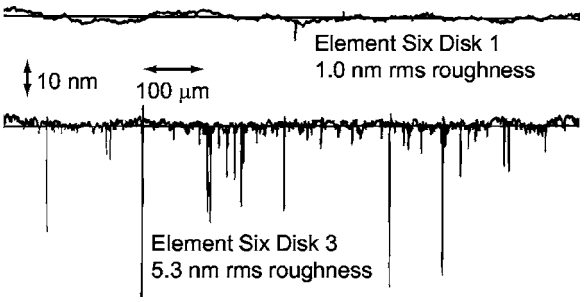

Fig. 11 Surface roughness of two 1 mm lengths measured with a Taylor-Hobson Talystep mechanical profiler. Note the different horizontal and vertical scales.

Figure 11 shows the range of roughness observed for the 10-mm disks from Element Six. The upper trace shows a relatively smooth surface with a root-mean-square roughness of 1.0 nm. The lower trace shows a surface with a similar outermost profile penetrated by many vertical scratches. The rms roughness for the lower trace is 5.3 nm. The range of surface roughness in Table 1 is sufficient to account for a significant fraction of the observed scatter. It should be possible to reduce the scatter by better surface finishing.

Visible photoluminescence in Figs. 9 and 10 provides information about defects in the diamond. The strong, sharp line at 573 nm is the 1332-cm^{-1} Raman peak characteristic of high quality diamond. Weak emission at 575 nm is attributed to a neutral nitrogen-vacancy complex, which is a nitrogen atom on a substitutional site adjacent to a carbon vacancy.[28] Weak emission at 637 nm is thought to arise from a nitrogen-vacancy complex with a negative charge. The underlying broad continuum could be associated with the nitrogen-vacancy complex, or might arise from dislocations that result from CVD diamond growth involving nitrogen. By comparison with the photoluminescence intensity of a single-crystal CVD diamond cutting tool from Element Six that was reported to have 1 to 2 ppm nitrogen, we estimate that the Element Six specimens in the present study contain 0.1 to 1 ppm nitrogen. Element Six material is grown in a gas mixture containing $\sim$1-ppm N_2. Single substitutional nitrogen measured by electron paramagnetic resonance in high quality Element Six material is reported to have a typical concentration in the range 0.3 to 3 ppm.[10] One surface of Apollo 5 (not shown) also exhibits weak emission near 734 nm, but no other specimens displayed this peak.

In conclusion, the 5×5-mm squares from Element Six had properties comparable to those of the best quality material reported by Element Six.[10] The absorption coefficient of Element Six disks with a diameter of 10 to 11 mm was 3 to 10 times greater than that of the squares. Apollo diamond absorbed about 30 times more energy than the best Element Six diamond, but one specimen from Apollo was comparable to the Element Six material. Absorption, loss of polarization, and optical scatter are sufficiently low for selected, properly oriented specimens of single-crystal, epitaxial CVD diamond to be used as heat spreading elements in the optical path of a solid state laser.

Acknowledgment

This work was supported by the Defense Advanced Research Projects Agency Microsystems Technology Office.

References

1. "Test method for absorptance of optical laser components," ISO/FDIS 11551, International Organization for Standardization, Geneva (1995).
2. U. Willamowski, D. Ristau, and E. Welsch, "Measuring the absolute absorptance of optical laser components," *Appl. Opt.* **37**, 8362–8370 (1998).
3. D. A. Orchard, P. D. Mason, E. J. McBrearty, and K. L. Lewis, "Laser calorimetry as a tool for the optimisation of MidIR OPO materials," *Proc. SPIE* **5273**, 379–387 (2003).
4. A. C. Victor, "Heat capacity of diamond at high temperature," *J. Chem. Phys.* **36**, 1903–1911 (1962).
5. D. L. Burk and S. A. Frieberg, "Atomic heat of diamond from 11° to 200°K," *Phys. Rev.* **111**, 1275–1282 (1958).
6. J. E. Graebner, "Measurements of specific heat and mass density in CVD diamond," *Diamond Relat. Mater.* **5**, 1366–1370 (1996).
7. U. Willamowski, T. Groß, D. Ristau, and H. Welling, "Calorimetric measurement of optical absorption at 532 nm and 1064 nm according to ISO/DIS 11551," *Proc. SPIE* **2870**, 483–494 (1996).
8. J. M. Bennett and J. H. Dancy, "Stylus profiling instrument for measuring statistical properties of smooth optical surfaces," *Appl. Opt.* **20**, 1785–1802 (1981).
9. P. C. Archibald and H. E. Bennett, "Scattering from infrared missile domes," *Opt. Eng.* **17**(6), 647–651 (1978).
10. H. P. Godfried, G. A. Scarsbrook, D. J. Twitchen, E. Houwman, W. G. M. Nelissen, A. J. Whitehead, C. E. Hall, and P. M. Martineau, "Optical quality diamond material," European Patent GB2411895 (14 Sep 2005); U.S. Patent Application 2004/0229464.
11. F. Peter, "Refractive indices and absorption coefficients of diamond between 644 and 226 mμ," *Z. Phys.* **15**, 358–368 (1923).
12. C. D. Clark, "The absorption edge spectrum of diamond," *J. Phys. Chem. Solids* **8**, 481–485 (1958).
13. J. Walker, "Optical absorption and luminescence in diamond," *Rep. Prog. Phys.* **42**, 1605–1659 (1979).
14. G. Davies, "The optical properties of diamond," in *Chemistry and Physics of Carbon*, Vol. **13**, P. L. Walker, Jr. and P. A. Thrower, Eds., pp. 1–143, Marcel Dekker, New York (1977).
15. *The Properties of Natural and Synthetic Diamond*, J. Field, Ed., Academic Press, London (1992).
16. *Properties and Growth of Diamond*, G. Davies, Ed., INSPEC, London (1994).
17. J. Wilks and E. Wilks, *Properties and Applications of Diamond*, Butterworth Heinemann, Oxford (1991).
18. J. Isberg, J. Hammersberg, E. Johansson, T. Wikström, D. J. Twitchen, A. J. Whitehead, S. E. Coe, and G. A. Scarsbrook, "High carrier mobility in single-crystal plasma-deposited diamond," *Science* **297**, 1670–1672 (2002).
19. E. P. Houwman, H. P. Godfried, C. E. Hall, J. Fraser, L. Daykin, S. J. Pope, and K. Mullaney, "Diamond solid etalons for high-stability DWDM wavelength-lockers," *Proc. 9th Eur. Conf. Opt. Commun./14th Intl. Conf. Integrated Opt. Opt. Fiber Commun.(ECOC-IOOC)* **3**, 500–501 (2003).
20. K. Meykens, K. Haenen, M. Nesládek, L. M. Stalls, C. S. J. Pickles, and R. S. Sussman, "Measurement and mapping of very low optical absorption of CVD diamond IR windows," *Diamond Relat. Mater.* **9**, 1021–1025 (2000).
21. S. E. Coe and R. S. Sussmann, "Optical, thermal, and mechanical properties of CVD diamond," *Diamond Relat. Mater.* **9**, 1726–1729 (2000).
22. C. S. J. Pickles, T. D. Madgwick, R. S. Sussmann, and C. J. H. Wort, "Optical performance of chemically vapour-deposited diamond at infrared wavelengths," *Diamond Relat. Mater.* **9**, 916–920 (2000).
23. T. P. Mollart, K. L. Lewis, C. S. J. Pickles, and C. J. H. Wort, "Factors affecting the optical performance of CVD diamond infrared optics," *Semicond. Sci. Technol.* **18**, S117–S142 (2003).
24. C. Piccirillo, G. Davies, A. Mainwood, S. Scarle, C. M. Penchina, T. P. Mollart, K. L. Lewis, M. Nesládek, Z. Remes, and C. S. J. Pickles, "Temperature dependence of intrinsic infrared absorption in natural and chemical-vapor deposited diamond," *J. Appl. Phys.* **92**, 756–763 (2002).
25. P. Dore, A. Nucara, D. Cannavò, G. De Marzi, P. Calvani, A. Marcelli, R. S. Sussmann, A. J. Whitehead, C. N. Dodge, A. J. Krehan, and H. J. Peters, "Infrared properties of chemical-vapor deposition polycrystalline diamond windows," *Appl. Phys. (N.Y.)* **37**, 5731–5736 (1998).
26. F. van Loon, A. J. Kemp, A. J. Maclean, S. Calvez, J. M. Hopkins, J. E. Hastie, M. D. Dawson, and D. Burns, "Intracavity diamond heatspreaders in lasers: the effects of birefringence," *Opt. Express* **14**, 9250–9260 (2006).
27. J. M. Bennett and L. Mattsson, *Introduction to Surface Roughness and Scattering*, Optical Society of America, Washington, D.C. (1989).
28. *The Properties of Natural and Synthetic Diamond*, J. Field, Ed., Chap. 2, Academic Press, London (1992).

Giorgio Turri graduated in 2001 at the Universita' degli Studi di Milano and gained his PhD in 2001 from the Politecnico di Milano. He began his research in experimental atomic and molecular physics, working at the Elettra Synchrotron in Trieste, Italy, and at the Advanced Light Source of the Lawrence Berkeley National Laboratory in California. His current interests are in optics and photonics, including laser calorimetry and characterization of lasing elements for solid state lasers. He focuses on spectroscopic properties of rare-earth-doped crystals and glasses.

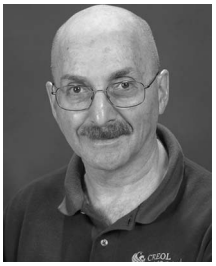

Michael Bass received a BS in physics from Carnegie-Mellon University and a PhD in physics from the University of Michigan in 1964, with thesis work on optical rectification. He was among the first to demonstrate homogeneous broadening in dye lasers. He was responsible for the statistical approach to understand laser-induced damage leading to recognition of electron avalanche breakdown as the intrinsic cause of this phenomenon. He is co-inventor of the $YAlO_3$ laser host and the use of fiber optics and lasers for the treatment of internal bleeding and tumors. He demonstrated the potential of such new solid state lasers as Cr:LiSAF and Nd:S-FAP. Areas now under study include materials for upconversion lasers and displays, high-average-power laser design, and thermal management for high-power lasers.

David Orchard was awarded a BA in physics from Oxford University, United Kingdom, in 1985, followed by a DPhil in laser physics from Oxford in 1989. He joined the Royal Signals and Radar Establishment (now part of QinetiQ) at Malvern the same year to work on development of mid-infrared laser sources and has now acquired extensive experience in the fields of laser physics and related optical systems. He is now a senior scientist at the Optronics Center at QinetiQ Malvern, with research interests in laser sources and applications, including development and characterization of engineered nonlinear materials for infrared generation and precision optical metrology.

James E. Butler leads a research group at the Naval Research Laboratory studying chemical events at a gas-solid interface during growth, etching, or catalysis. He has published more than 210 papers in experimental chemical physics, including elementary reaction dynamics, chemical kinetics, laser photochemistry, spectroscopy, optical diagnostics, surface chemistry, and chemical vapor processing. He is an expert on the chemical vapor deposition of diamond and has served as a technical advisor to government programs on diamond. He received an BS in chemistry from Massachusetts Institute of Technology in 1966 and a PhD in chemical physics from The University of Chicago in 1972. He joined the Naval Research Laboratory in 1975.

Daniel C. Harris is a senior scientist and Esteemed Fellow at the Naval Air Systems Command, China Lake, California, where he is responsible for infrared window materials research and development programs. He has degrees in chemistry from Massachusetts Institute of Technology in 1968 and California Institute of Technology in 1973. He is the author of *Materials for Infrared Windows and Domes* and a series of widely used textbooks in analytical chemistry.

C. Martin Stickley received electrical engineering degrees from Cincinnati, Massachusetts Institute of Technology, and Northeastern University. As a Lieutenant in the U.S. Air Force, he built the Air Force's first laser in 1960. He served two tours at the Defense Advanced Research Project Agency, was the first director of the Laser Fusion Office in the Department of Energy, was a senior vice president of the BDM Corporation for eleven years, and associate director of CREOL at the University of Central Florida for 12 years. He is a Fellow of the Optical Society of America and a Life Fellow of IEEE.

Biographies and photographs of other authors not available.